

Measuring thin film elastic modulus using a micromachined cantilever bending test by nanoindenter

Changchun Hsu
National Tsing Hua University
Power Mechanical Engineering Department
Hsinchu, Taiwan

Chingfu Tsou
Feng Chia University
Department of Automatic Control Engineering
Taichung, Taiwan

Weileun Fang
National Tsing Hua University
Power Mechanical Engineering Department
Hsinchu, Taiwan
E-mail: fang@pme.nthu.edu.tw

Abstract. It is convenient to characterize thin film material properties using commercially available nanoindentation systems. This study aims to discuss several considerations while determining the thin film elastic modulus by means of a microcantilever bending test using a commercial nanoindentation system. The measurement results are significantly improved after: 1. the indentation of the film during the test is considered and corrected, and 2. the boundary effects are considered in the model by finite element method. In application, the elastic modulus of electroplating nickel film 11 μm thick was characterized. © 2007 Society of Photo-Optical Instrumentation Engineers. [DOI: 10.1117/1.2778431]

Subject terms: elastic modulus; thin film; nanoindenter.

Paper 06067RR received Oct. 6, 2006; revised manuscript received Apr. 17, 2007; accepted for publication May 8, 2007; published online Sep. 21, 2007.

1 Introduction

The elastic modulus is an important mechanical property for structure design. The elastic modulus of thin film materials is also important for the design of microelectromechanical system (MEMS) devices. The mechanical properties of thin film materials may not be the same as that of the bulk ones. Moreover, the mechanical properties of thin film materials usually vary with the fabrication process, film thickness, etc. Various static load-deflection tests have been studied to determine the elastic modulus of thin films precisely; for instance, the tensile test,^{1–10} three point bending test,¹¹ indentation test,^{3,12–15} bulge test,^{16,17} bending beam test,^{14,15,18–20} etc. However, there are no standard testing methods so far. Among these approaches, the sample preparation and the test setup are two major considerations for tensile tests.^{1,2,11,16,17} In addition, the nanoindentation approach^{12,13} is significantly influenced by the substrate and roughness of the sample.

The bending beam test is a convenient technique to measure the elastic modulus, the yield strength, and the fracture toughness of thin films.^{18–20} The test stand requires a microprobe to apply a load in the range of μN , and a displacement sensor with a resolution of subnanometers is also necessary. Presently, the commercialized nanoindentation system^{18,19} and atomic force microscopy (AFM) system^{21,22} have been employed for the bending micromachined beam test. The loading probe of the nanoindentation system is much stiffer than that of the AFM, so that the relation of load deflection is less complicated. In short, the commercial nanoindentation system not only provides the capabilities of measuring hardness, elastic modulus, friction coefficient, and adhesion force, but also meets the requirements for microcantilever bending test. Moreover, the wafer-level test

is available using the commercial nanoindentation system. The distribution of the thin film mechanical properties on the wafer surface can also be characterized. Thus, the nanoindentation system has the potential to become the most powerful instrument for the characterization of thin film mechanical properties.

This study has employed the nanoindentation system to determine the thin film mechanical properties using the bending beam test, as shown in Fig. 1. Loading and sensing were performed using a commercial nanoindentation system. During the bending test, the probe was placed at various locations of cantilever. After measuring the displacement δ of the probe under specific load P and at a particular point, the elastic modulus of the thin film can be determined from

$$E = \frac{4L_e^3}{wt^3} \cdot \frac{P}{\delta}, \quad (1)$$

where w and t are the width and the thickness of the cantilever beam, respectively. In addition, L_e is the equivalent beam length between the loading position and the fixed end of cantilever. In Eq. (1), the parameter P/δ is the stiffness of test beam associated with the length L_e , and was determined from the slope of the load-displacement curve.

This study further investigates various issues that may influence the elastic modulus determined from the bending beam test by a nanoindentation system. For instance, the thin film cantilever may experience not only flexible deflection but also indentation when loaded by the indenter. In addition, the boundary conditions of the micromachined cantilever also need to be considered in the model. Thus, the ideal clamped boundary conditions employed in Eq. (1) are modified. Thus, the elastic modulus extracted from the bending beam test using the nanoindentation system is significantly improved.

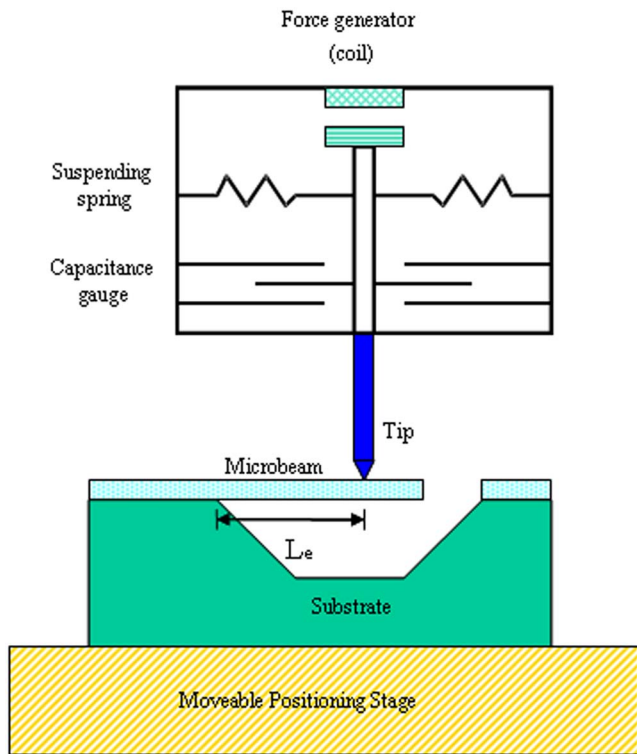


Fig. 1 The schematic illustration of microcantilever bending test by nanoindenter.

2 Experiments and Results

In this study, bulk micromachining was employed to fabricate test cantilevers. After that, a commercial nanoindentation system (Nanoindenter XP, MTS Instruments) was used to perform the load-deflection test for cantilevers. Thus the elastic modulus of thin film was extracted from the load-deflection relations.

2.1 Sample Preparation

Electroplated thin nickel (Ni) film was employed as the material for case study. The fabrication process to prepare the test sample is shown in Fig. 2. First, an insulation SiO_2 layer was thermally grown on a (100) Si wafer, and then the titanium (Ti) and Ni films were deposited as adhesive layers and seed layers, respectively, as shown in Fig. 2(a). After that, the thick photoresist was spun and patterned on a silicon substrate, and then the Ni film was electroplated, as illustrated in Fig. 2(b). The photoresist was removed for the lift-off process and the adhesive and seed layers were removed by wet etching, as shown in Fig. 2(c). Finally, the Ni cantilevers were free suspended on the substrate after the bulk silicon etching by N_2H_4 , as shown in Fig. 2(d). Figure 2(e) shows the scanning electron microscope (SEM) photograph of various typical micromachined Ni cantilever beams. The planar dimensions of the cantilever were measured using a commercial measuring microscope. A submicron resolution was achieved using an optical linear scale. The thickness of the cantilever was measured using a contact surface profiler before bulk silicon etching. Since the etching selectivity of Si over Ni is extremely large in N_2H_4 , the thickness variation of the Ni film was much less than

(a) Thermal oxidation and Evaporation Ti/Ni



(b) Pattern & electroplating Ni



(c) Lift off & remove Ti/Ni, SiO_2



(d) Wet etching



(e) Typical microfabricated cantilever

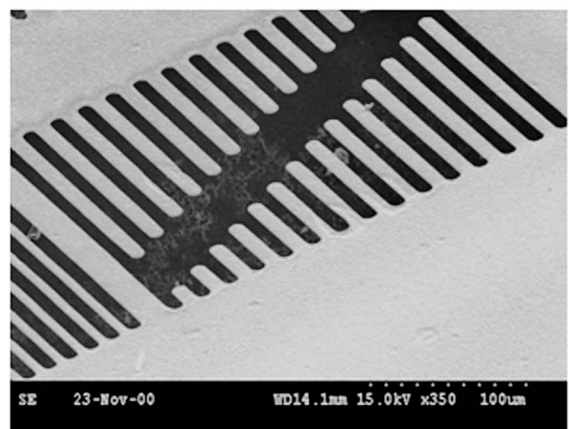


Fig. 2 (a) to (d) The fabrication process steps of the electroplated micromachined cantilever, and (e) the SEM photograph of typical electroplated Ni test cantilever array.

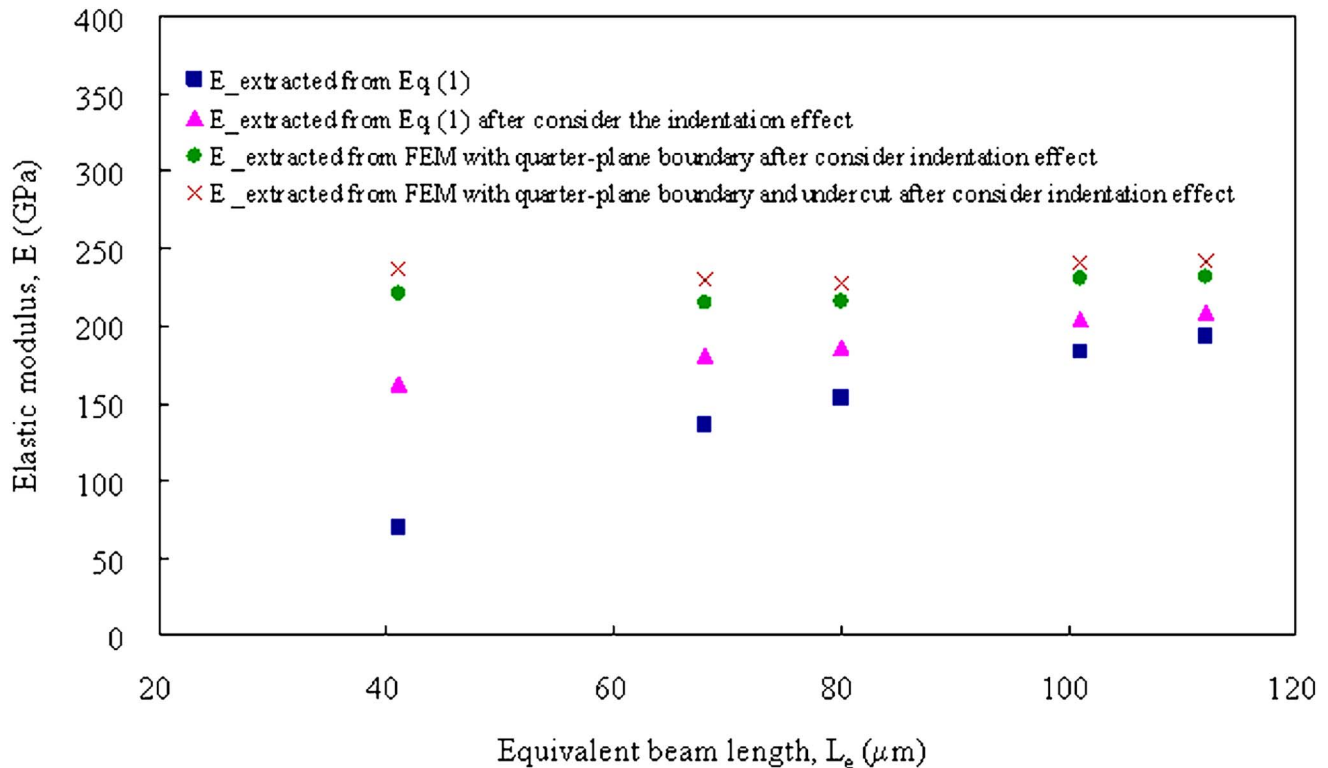


Fig. 3 The elastic modulus E determined after the microcantilever bending test for different equivalent beam lengths L_e .

0.1 μm after bulk silicon etching. The micromachined cantilevers were 8 μm wide and 11 μm thick, and their lengths ranged from 20 to 150 μm . The N_2H_4 etchant has a smaller etching selectivity of (111) to (100) crystal planes, and the undercut of (111) planes during bulk silicon etching cannot be ignored. Meanwhile, the boundary conditions of the cantilever were influenced due to the undercut of (111) planes. In this study, it took 30 min to fully suspend the test cantilever, and its boundary was undercut for 4 μm . Before the bending test, an optical interferometer was used to measure the deflection of the micromachined cantilever resulting from the residual stresses. The measured out-of-plane deformation along the beam length is very small, so that the residual stress effect is neglected in this experiment.

2.2 Measurement and Results

As shown in Fig. 1, the commercial nanoindentation system mainly consisted of a magnetic loading actuator, a capacitive displacement sensor, a probe, and supporting springs.^{12,13} Thus, the load and displacement can be precisely controlled and measured during the experiment. The force resolution of the loading actuator is approximately at sub- μN load scale, and the displacement sensing resolution of the capacitive sensor is within nanometer length scale. In addition, the displacement resolution of a moving stage is approximately $\pm 1.5 \mu\text{m}$. This study employed the constant-load mode of the system during the load-deflection test. The probe with a Berkovich triangular pyramidal tip was used to apply a prescribed load P ($P=0.098 \text{ mN}$) on the test beam. In the load-deflection test, the micromachined Ni cantilever was 150 μm long. The loads were applied at five different positions along the beam length of the same can-

tilever; and the equivalent beam length L_e ranged from 41 to 112 μm , controlled by an xy position stage. According to the strain hardening effect, the elastic modulus of thin film near the loading region could be increased after the bending test. To prevent the influence of the strain hardening effect on the elastic modulus determined from the bending test, the loading positions were moved from the free end to the anchored end of the beam. According to existing approaches,¹⁸⁻²⁰ the elastic modulus of the film was extracted from Eq. (1) based on the prescribed load P and the measured beam deflection δ . As indicated by the square dots in Fig. 3, the elastic modulus extracted from Eq. (1) was not a constant, but varied significantly with the equivalent beam length L_e . Apparently, this is a critical problem for the bending cantilever approach.

3 Discussion

The variation of elastic modulus with the equivalent beam length, as indicated by the square dots in Fig. 3, resulted from various effects. To accurately determine the thin film elastic modulus using the bending test of the microcantilever, these effects are investigated and discussed as follows.

3.1 Indentation Effects

The probe with a Berkovich triangular pyramidal tip will lead to a residual indent on the thin film surface after a conventional indentation test.²³ Since the "constant-load" mode of nanoindenter was employed in the test, the surface of the cantilever would experience a constant prescribed load P from the Berkovich tip. The surface would be indented by the sharp triangular tip. In other words, the probe will lead to not only the elastic deformation d_e of cantilever

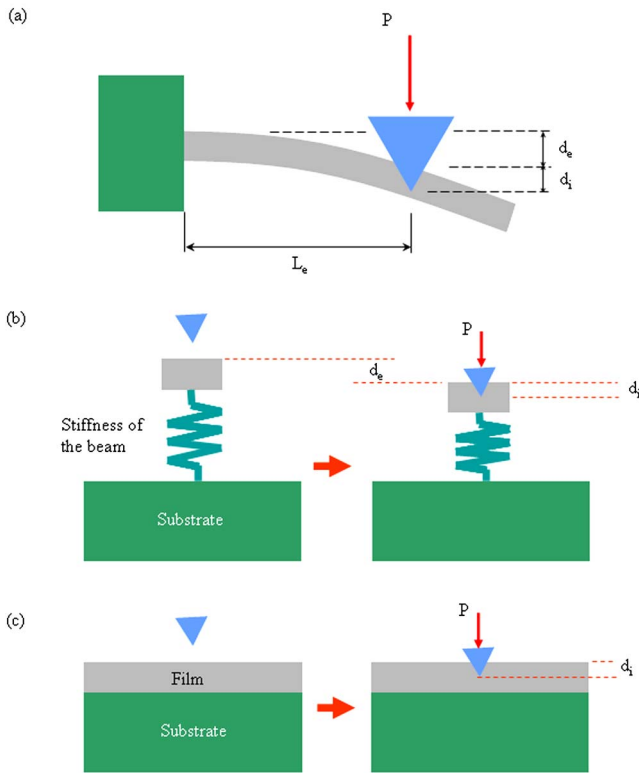


Fig. 4 The schematic of (a) the indentation effect on micromachined cantilever during bending test, (b) the equivalent load-deflection beam model, and (c) the equivalent indentation model.

but also the indentation of the film d_i during the load-deflection test, as illustrated in Fig. 4(a). The equivalent load-deflection and indentation models are illustrated in Figs. 4(b) and 4(c), respectively. Briefly, no matter whether the film was rigidly supported or freely suspended, it would experience the same magnitude of reaction P at the contact point. Since the rigidly supported film and freely suspended film were electroplated simultaneously, they had the same material properties and the same penetration depth d_i under a constant load P . Thus, this study employed the conventional indentation test on the unreleased film to determine the penetration depth d_i of the suspended cantilever. The typical load-deformation curves of six indent points for the rigidly supported Ni film are demonstrated in Fig. 5. The indenter load is increased from zero (S) to a certain maximum value P_{max} , and then gradually decreased to zero.

Thus, the net displacement of the probe δ measured by the nanoindentation system consisted of the elastic deformation d_e of the cantilever and the indent of the film d_i . In this regard, the exact elastic beam deflection d_e was smaller than the displacement of the probe δ measured by the indentation system. Based on the elastic deflection of the test cantilever, the corrected elastic modulus E_c is expressed as

$$E_c = \frac{4L_e^3}{wt^3} \cdot \frac{P}{\delta - d_i} \quad (2)$$

If the indentation effect is ignored, the percentage error of the elastic modulus is

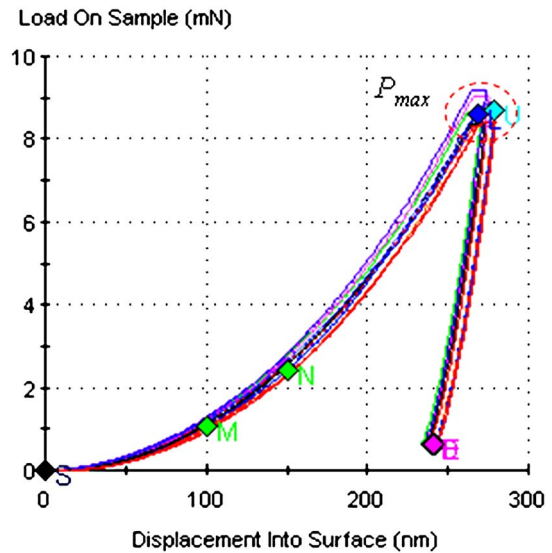


Fig. 5 The load-deflection curve measured from indentation tests of unreleased film.

$$\frac{E - E_c}{E_c} = \frac{-d_i}{d_i + d_e} \quad (3)$$

Since a constant load P was prescribed to apply to the beam during the load-deflection tests, the indentation depth d_i was also a constant. However, the elastic deflection d_e as well as the probe displacement δ is decreased for a smaller L_e . According to Eq. (3), the elastic modulus extracted from the bending beam technique has a larger error for a smaller L_e (i.e., a smaller elastic deflection d_e) if the indentation effect is ignored. Thus, the elastic modulus extracted from the bending test of shorter equivalent beam length L_e is smaller. This explanation agrees qualitatively with the measurement results of square dots in Fig. 3.

According to the conventional Ni film indentation test, the penetration depth d_i corresponding to P ($=0.098$ mN) was measured to be 20 nm. Thus, the corrected elastic modulus was extracted from Eq. (2) after the load-deflection test. The elastic modulus of Ni film measured at five different lengths L_e after considering the indentation effect are also depicted in Fig. 3. The data points were the average of five different measurements. As represented by the triangular dots, the elastic moduli determined after considering the indentation effect ranged from 209 to 162 GPa when the beam length decreased from 112 to 41 μm . By comparison, the elastic moduli of square dots ranged from 193 to 69 GPa for the same equivalent beam lengths. Thus, after considering the indentation effect, the elastic modulus extracted from the load-deflection test has a variation of 22% when L_e ranged from 41 to 112 μm .

3.2 Boundary Effects

In addition to the indentation effect, the boundary conditions also need to be considered in the model. The schematic illustration in Fig. 6(a) shows the physical model of an ideal cantilever beam, and the displacement and slope are fixed along the whole boundary (half-plane boundary).

Table 1 Available elastic modulus of Ni film fabricated and determined from various approaches.

References	Test method	Specimen dimensions	E (GPa)	Conditions of electroplating
Present study	Cantilever bending	Width \times thickness: $8 \times 11 \mu\text{m}$	235	Sulfamate bath, 50°C current density: 5 mA/cm^2
	Nano-indentation	Thickness: $11 \mu\text{m}$	271	
Ref. 3	Tensile comp.	High: 1.66 mm Diameter: 1.0 mm	160 ± 1.0	Sulfamate bath, 50°C , current density: 50 mA/cm^2
			156 ± 9.3	Sulfamate bath, 50°C , current density: 20 mA/cm^2
Ref. 4	Tensile	Width \times thickness: $200 \times 200 \mu\text{m}$	176 ± 30	Sulfamate bath 3rd LIGA multi-project run coordinated through MCNC
Ref. 5	Tensile	Width \times length: $20 \times 300 \mu\text{m}$ Thickness: 120 to $200 \mu\text{m}$	202	Sulfamate bath, 50°C , current density: 1 A/dm^2
	Vibration	Width \times length: $300 \times 1000 \mu\text{m}$ Thickness: 120 to $200 \mu\text{m}$	205	
Ref. 6	Tensile	Width \times thickness: $14 \times 6 \mu\text{m}$	231 ± 12	NA
Ref. 7	Tensile	Length: 5 to $25 \mu\text{m}$ Width \times thickness: $5 \times 50 \mu\text{m}$	189	Sulfamate bath, 50°C
Ref. 8	Tensile	Length \times width \times thickness $600 \times 15 \times 50 \mu\text{m}$	99.5 to 125.2	UV-LIGA process testing at 300 to 573 K
Ref. 9	Tensile	Full test specimens: $2 \times 17 \text{ mm}$	160 ± 20	Sulfamate bath, 50°C current density: 50 mA/cm^2
Ref. 10	Tensile	Width: $200 \mu\text{m}$ Thickness: 100 to $200 \mu\text{m}$	180 ± 24	2nd LIGA fabrication run for NSWC
Ref. 14	Microbridge bending	Length: 1045 to $1541 \mu\text{m}$ Width: 195 to $940 \mu\text{m}$ Thickness: $3.7 \mu\text{m}$	190.1	NA
	Nano-indentation	NA	186.8 ± 7.5	NA
Ref. 15	Cantilever bending	Length: $1000 \mu\text{m}$ Width \times thickness: $160 \times 160 \mu\text{m}$	214	Watts bath, 45°C current density: 30 mA/cm^2
			125	Sulfamate bath, 55°C current density: 30 mA/cm^2
	Nano-indentation	Thickness: $160 \mu\text{m}$	230	Watts bath, 45°C current density: 30 mA/cm^2
			133	Sulfamate bath, 55°C current density: 30 mA/cm^2

However, the boundary of micromachined cantilever Fig. 6(a) was fixed to the substrate only at its bottom surface (quarter-plane boundary), as illustrated in Fig. 6(b). Hence, the real boundary condition of the micromachined cantilever is not exactly the same as that of the conventional half-plane boundary.²⁴ In addition, the influence due to the undercut of the cantilever at its boundary during the bulk silicon etching was also investigated. Figure 6(c) illustrates the boundary undercut of the microcantilever.

This study employed the commercial software, ANSYS, to attempt to quantitatively evaluate the boundary effects. Based on the illustration in Fig. 6(b), the finite element

model consisted of a thin film that is partially fixed at the bottom surface.²⁴ The square and triangular dots in Fig. 3 represent the results based on the ideal half-plane boundary cantilever in Fig. 6(a), whereas the circular dots in Fig. 3 represent the results based on the quarter-plane boundary cantilever in Fig. 6(b). The elastic modulus of circular dots was extracted from the finite element model but not Eq. (1). By comparing the results of square and circular dots, the difference of these two cases was increased from 11 to 36% when the length L_e decreased from 112 to $41 \mu\text{m}$. Hence, the quarter-plane boundary effect has significant influence for a smaller L_e . After considering the indentation and

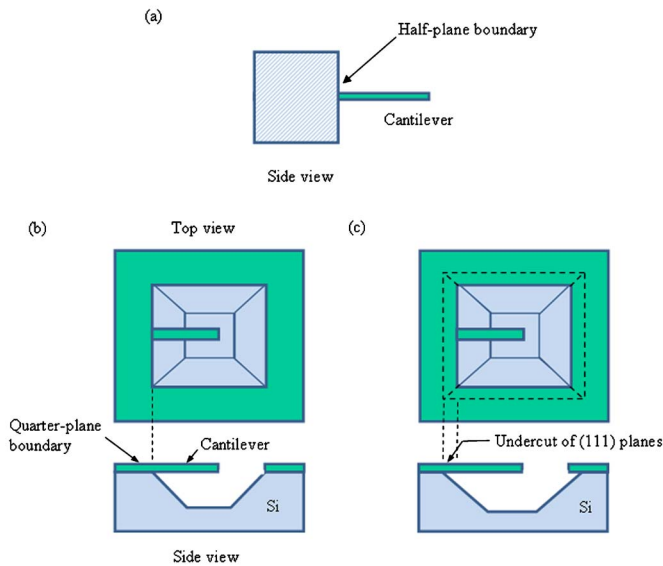


Fig. 6 The schematic illustrations of (a) the ideal half-plane boundary, (b) the real quarter-plane boundary, and (c) the boundary undercut.

quarter-plane boundary effects, the variation of elastic modulus extracted from the load-deflection test drops to 7% when L_e ranges from 41 to 112 μm . Moreover, the cross dots in Fig. 3 represent the elastic modulus extracted from the FEM model with the cantilever shown in Fig. 6(c). In this case, the cantilever was not fixed to the quarter-plane boundary [as indicated in Fig. 6(b)] but fixed to the suspended plate from the undercut. The difference of the elastic modulus was near 4 to 7% when the boundary of the cantilever was undercut for 4 μm .

In short, a more accurate elastic modulus can be extracted from the bending beam test by considering the indentation and boundary effects. Further, the elastic modulus will not vary with the loading position (i.e., the equivalent beam length) of the test. After considering the indentation and boundary effects, the elastic modulus of 11- μm -thick Ni film determined from the bending beam test is significantly increased from 69 to 237 GPa when length L_e is 41 μm . Moreover, the elastic modulus is also increased from 193 to 242 GPa for a 112- μm -long L_e . As a comparison, the elastic modulus determined directly from the conventional nanoindentation test was 271 GPa. Other available elastic modulus of Ni film determined from various approaches are listed in Table 1.^{3–10,14,15}

4 Conclusions

The primary contribution of this study is to consider the indentation depth of thin film during a micromachined cantilever bending test. Thus, the elastic modulus determined using this approach will not significantly vary with the location of the applied load. Moreover, the study also considers the effects due to the quarter-plane boundary and the overetching of the (111) crystal planes during the bending beam test. The finite element analysis has been employed to investigate the boundary effects. In application, the elastic modulus of an 11- μm -thick Ni film was fabricated and characterized. The elastic modulus determined from the

present bending beam approach ranged from 228 to 242 GPa. As a comparison, the elastic modulus determined from the conventional nanoindentation test was 271 GPa. In summary, after considering the indentation and boundary effects, the present study significantly improves the elastic modulus extracted from the cantilever bending test using a nanoindentation system. Because this approach is very simple and straightforward, it can act as a supplement to other elastic modulus measurement techniques.

Acknowledgments

This project was (partially) supported by National Science Council, Taiwan, under contract number 92-2212-E-007-052. The authors are grateful to the National Science Council Central Regional MEMS Research Center (Taiwan), Nano Facility Center of National Chiao-Tung University (Taiwan), and National Nano Device Laboratory (Taiwan), for providing the fabrication facilities.

References

1. W. N. Sharpe, Jr., B. Yuan, and R. Vaidyanathan, "Measurements of Young's modulus, Poisson's ratio, and tensile strength of polysilicon," *Proc. IEEE MEMS'97*, pp. 424–429 (1997).
2. H. Ogawa, Y. Ishikawa, and T. Kitahara, "Measurements of stress-strain diagrams of thin films by a developed tensile machine," *Proc. SPIE* **2880**, 272–277 (1996).
3. T. Buchheit, T. Christenson, D. Schmale, and D. Lavan, "Understanding and tailoring the mechanical properties of LIGA fabricated materials," *Proc. MRS Symp.* **546**, 121–126 (1998).
4. W. N. Sharpe, Jr., D. A. LaVan, and R. L. Edwards, "Mechanical properties of LIGA-deposited nickel for MEMS transducers," *Proc. Transducers '97*, pp. 607–610 (1997).
5. E. Mazza, S. Abel, and J. Dual, "Experimental determination of mechanical properties of Ni and Ni-Femicrobars," *Microsyst. Technol.* **2**, 197–202 (1996).
6. S. Greek and F. Ericson, "Young's modulus, yield strength and fracture strength of microelements determined by tensile testing," *Proc. MRS Symp.* **518**, 51–56 (1998).
7. J. Lou, S. Allameh, T. Buchheit, and W. O. Soboyejo, "An investigation of the effects of thickness on mechanical properties of LIGA Nickel MEMS structures," *J. Mater. Sci.* **38**, 4129–4135 (2003).
8. Y. Isono, J. Tada, T. Watanabe, T. Unno, T. Toriyama, and S. Sugiyama, "Elevated temperature tensile/creep test of UV-LIGA nickel thin film for design of high-density micro connector," *Proc. 12th Intl. Conf. Solid-State Sensors Actuators* **1**, 456–460 (2003).
9. T. Christenson, T. Buchheit, D. Schmale, and R. Bourcier, "Mechanical and metallographic characterization of LIGA fabricated nickel and 80% Ni-20% Fe permalloy," *Proc. MRS Symp.* **518**, 185–190 (1998).
10. K. J. Hemker and H. R. Last, "Microsample tensile testing of LIGA nickel for MEMS applications," *Mater. Sci. Eng. A* **319–321**, 882–886 (2001).
11. A. Rouzaud, E. Barbier, J. Ernoult, and E. Quesnel, "A method for elastic modulus measurements of magnetron sputtered thin films dedicated to mechanical applications," *Thin Solid Films* **270**, 270–274 (1995).
12. W. C. Oliver and G. M. Pharr, "An improved technique for determining hardness and elastic modulus using load and displacement sensing indentation experiments," *J. Mater. Res.* **7**, 1564–1583 (1992).
13. G. M. Pharr and W. C. Oliver, "Measurement of thin film mechanical properties using nanoindentation," *MRS Bull.* **7**, 28–33 (1992).
14. Z. M. Zhou, Y. Zhou, C. S. Yang, J. A. Chen, G. F. Ding, W. Ding, M. J. Wang, and Y. M. Zhang, "The evaluation of Young's modulus and residual stress of nickel films by microbridge testings," *Meas. Sci. Technol.* **15**, 2389–2394 (2004).
15. L. S. Stephens, K. W. Kelly, S. Simhadri, A. B. McCandless, and E. I. Meletis, "Mechanical property evaluation and failure analysis of cantilevered LIGA nickel microposts," *J. MEMS* **10**, 347–359 (2001).
16. M. G. Allen, M. Mehregany, R. T. Howe, and S. D. Senturia, "Microfabricated structures for the in situ measurement of residual stress, Young's modulus, and ultimate strain of thin films," *Appl. Phys. Lett.* **51**, 241–243 (1987).
17. D. Maier-Schneider, J. Maibach, E. Obermeier, and D. Schneider, "Variations in Young's modulus and intrinsic stress of LPCVD-Polysilicon due to high temperature annealing," *J. Micromech. Microeng.* **5**, 121–124 (1995).
18. W. D. Nix, "Mechanical properties of thin films," *Metal. Trans. A* **20A**, 2217–2245 (1989).

19. T. P. Weihs, S. Hong, J. C. Bravman, and W. D. Nix, "Mechanical deflection of cantilever microbeams: a new technique for testing the mechanical properties of thin films," *J. Mater. Res.* **3**, 931–942 (1988).
20. S. Johansson, J. A. Schweitz, L. Tenerz, and J. Tiren, "Fracture testing of silicon microelements in situ in a scanning electron microscope," *J. Appl. Phys.* **66**, 4799–4803 (1988).
21. J. D. Holbery, V. L. Eden, M. Sarikaya, and R. M. Fisher, "Experimental determination of scanning probe microscope cantilever spring constants utilizing a nanoindentation apparatus," *Rev. Sci. Instrum.* **71**, 3769–3776 (2000).
22. D. Saya, K. Fukushima, H. Toshiyoshi, G. Hashiguchi, H. Fujita, and H. Kawakatsu, "Fabrication of single-crystal Si cantilever array," *Sens. Actuators, A* **95**, 281–287 (2002).
23. B. Bhushan, *Handbook of Micro/Nano Tribology*, 2nd ed., CRC Press, Boca Raton, FL (1998).
24. W. Fang and J. A. Wickert, "Determining mean and gradient residual stresses in thin films with micromachined structures," *J. Micromech. Microeng.* **6**, 301–309 (1996).

Biographies and photographs of the authors not available.